10.1109/ULTSYM.2014.0655

An Ultrasound-Based Noninvasive Neural Interface to the Retina

Projection Algorithm and Frontend Integrated Circuit Architecture

Xun Wu, Mohit Kumar, and Ömer Oralkan
Department of Electrical and Computer Engineering
North Carolina State University
Raleigh, NC 27606, USA
xwu12@ncsu.edu, mohitk@ncsu.edu, ooralka@ncsu.edu

***Abstract*—Focused ultrasound (FUS) is emerging as a promising technology for neural stimulation. In this study, we demonstrate the algorithm and the frontend integrated circuit (IC) architecture design for an ultrasound-based noninvasive neural interface to the retina. A digital image is provided as the input to the system, and the system calculates the excitation signal for each element in a 2D transducer array. With each element being excited accordingly, the array can "project" the image onto the retina as an ultrasound field pattern (USFP). The algorithm is based on the fast Fourier transform (FFT), which makes real-time implementation feasible.**

Keywords—FUS; Neural stimulation; Noninvasiveness; FFT

I. Introduction

A previous study showed that FUS could create neural responses in the retina that are similar to those stimulated by natural visual inputs [1]. Compared to electrical neural stimulation, which requires implantation of a microelectrode array, an invasive interface to the retina, FUS is a noninvasive method and can potentially provide higher spatiotemporal resolution.

In our envisioned system, a 2D capacitive micromachined ultrasonic transducer (CMUT) array with integrated electronics is placed in front of the eye to project a dynamically updated USFP onto the retina (Fig. 1). A projection algorithm is used to calculate the excitation pattern, which is a set of signals to be applied to the elements in the array to generate the desired USFP. An iterative algorithm with high computational complexity has been previously developed [2]. In this paper, we develop a new algorithm that has reduced computational complexity and facilitates real-time implementation. A frontend IC architecture is also designed to provide the actual excitation signals.

The current design is devised for use with a circularly shaped 2D CMUT array and the excitation signal to each element is assumed to be a unipolar square wave for simpler hardware implementation. The system parameters for the design are listed in Table I. Ultrasound field simulations are performed using Field II [3], [4]. Simulated data for circuits are obtained using transistor-level simulations (Cadence Design Systems, San Jose, CA). The performance of the algorithm is quantitatively analyzed for different cases.

This work was supported by the Defense Advanced Research Projects Agency (DARPA) under grant D13AP00043.

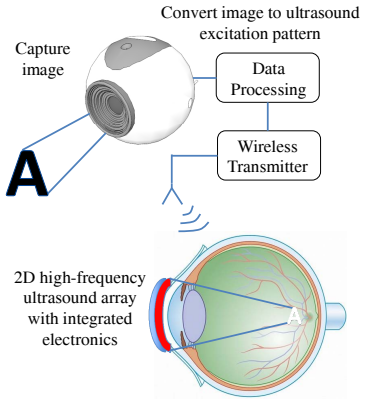

Figure 1. Overall architecture of the system

TABLE I. System Parameters

Center frequency	40 MHz	Array size	128× 128
Projection distance	22 mm	Element pitch	130 μm

Projection distance is the distance between the plane that the array lies in and the target plane. This distance is set according to the average distance between the front surface of the eyeball and the retina.

II. The Projection Algorithm

The input of the algorithm is a digital image $P(m,n)$ ($m = 1,\ldots M$, $n = 1,\ldots N$) and the size of the target plane. Each pixel in the image defines a target on the plane (Fig. 2(a)). The algorithm is designed to calculate the excitation pattern for the array to "project" the image onto the target plane as a USFP.

The 2D Fourier transform (FT) relates the transducer aperture function $S(x_0, y_0)$ with the resultant field pattern $P(x, y, z)$ on an x-y plane in the far field (Fig. 2(b)) [5]:

$$P(x,y,z) = \frac{1}{\lambda z} F\{S(x_0,y_0)\}\Big|_{u=\frac{x}{\lambda z}, v=\frac{y}{\lambda z}} \quad (1)$$

So, if given a certain field pattern, we can calculate the corresponding aperture function using a 2D inverse Fourier Transform (IFT):

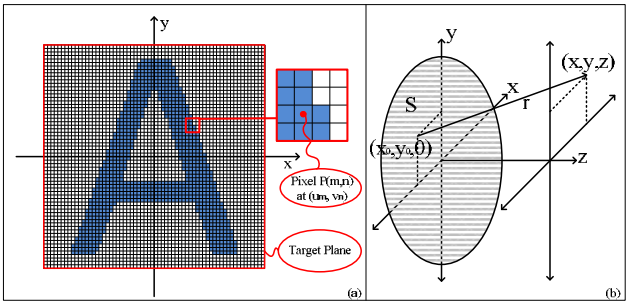

Figure 2. (a) An example of the digital image as the input to the system. (b) Geometry of the coordinate system.

$$S(x_0, y_0) = \frac{1}{\lambda z} F^{-1}\{P(u,v,z)\}\Big|_{x=\frac{x_0}{\lambda z}, y=\frac{y_0}{\lambda z}} \quad (2)$$

A. *FFT-based projection algorithm*

According to (2), a discrete algorithm can be derived for the presented case:

$$S(x_0, y_0) = \frac{1}{\lambda z} \sum_{m=1}^{M} \sum_{n=1}^{N} P(m,n) \exp(j2\pi(u_m \frac{x_0}{\lambda z} + v_n \frac{y_0}{\lambda z})) \quad (3)$$

With (3), which is very similar to a 2D inverse discrete Fourier transform (IDFT), the excitation signal for each element in the array can be calculated to project arbitrary images. Computational complexity can be reduced for (3) by applying the FFT with the following two constraints imposed on relevant parameters.

Constraint 1: The size of the image is the same as the array size (M = N = 128 in our case).

Constraint 2: The size of the target plane is $\lambda \times$ (*projection distance*) / (*element pitch*).

As a result, the computational complexity is reduced from $O(N^4)$ to $O(N^2 \log_2 N)$.

A prerequisite for the derivation of the algorithm is that the target plane must be placed in the far field of the transducer so that (2) holds. If the target plane is in the near field, a spherical delay pattern can be overlapped with the calculated excitation pattern to bring the far field "closer" so that (2) still holds.

B. *Quantization of the excitation signals*

The complete set of excitation signals calculated with the algorithm involves arbitrary amplitudes and phases. This introduces significant difficulty in implementing the algorithm in hardware. In order to simplify the hardware implementation, we quantized excitation signals both in amplitude and phase.

Different numbers of quantization levels have been tested. Both the amplitudes and phases have been uniformly quantized to four, eight, sixteen, and thirty-two levels. Quantitative analysis has been performed on simulated field patterns to explore the tradeoff between the number of quantization levels and projected image quality to guide the hardware implementation.

C. *Simulations and quantitative analysis*

Twenty-six 128×128 images of Calibri font letters from "A" to "Z" are used as inputs. These images are chosen to be bit maps (each pixel is either 0 or 1) for more convenient quantitative analysis of the performance. The targets corresponding to the pixel value of "1" form a focused area (Fig. 5(a)). After the excitation pattern is calculated with the FFT projection algorithm, it is quantized uniformly and then fed to the array defined in Field II. The root-mean-square (RMS) pressure at each target pixel is calculated and stored in a 2D array, which is then normalized, compressed, and displayed as an image for visualization of the simulation results. Two metrics are used to evaluate the performance of the algorithm in creating a pattern.

1. Coverage: Assume that there are F targets corresponding to the pixel value of "1", and E of them lie within the area surrounded by the -10-dB contour of the RMS pressure distribution. Coverage is defined as E/F.

2. Contrast-to-noise ratio (CNR): The CNR is defined as:

$$CNR = \frac{< P_{focused} > - < P_{unfocused} >}{\sqrt{\sigma^2_{focused} + \sigma^2_{unfocused}}}$$

$< P_{focused} >$ and $\sigma^2_{focused}$ are the mean and variance of the RMS pressure in the focused area, $< P_{unfocused} >$ and $\sigma^2_{unfocused}$ are those outside the focused area [6].

The simulation results for the letter "A" with different numbers of quantization levels are shown in Fig. 3. The average coverage and CNR for the twenty-six letters from "A" to "Z" are shown in Table II and Table III.

According to Table II and III, as expected, the performance of the algorithm improves as the number of quantization levels increases. However, generating a larger number of quantization levels increases the complexity of hardware implementation. We decided to use eight levels of amplitudes and eight levels

TABLE II. AVERAGE COVERAGE

Number of amplitudes →

Number of phases ↓	4	8	16	32	2^{64}
4	0.9444	0.9777	0.9892	0.9961	0.9974
8	0.9490	0.9829	0.9946	0.9987	0.9998
16	0.9571	0.9879	0.9958	0.9996	0.9999
32	0.9565	0.9872	0.9962	0.9996	0.9999
2^{64}	0.9564	0.9880	0.9964	0.9996	1.0000

TABLE III. AVERAGE CNR

Number of amplitudes →

Number of phases ↓	4	8	16	32	2^{64}
4	2.8050	3.4804	3.9057	4.2791	4.4755
8	3.0140	3.8521	4.3964	4.9444	5.2836
16	3.1329	4.0334	4.5993	5.2182	5.5923
32	3.1474	4.0644	4.6498	5.2827	5.6764
2^{64}	3.1522	4.0704	4.6588	5.2956	5.7016

Number of phases ↓

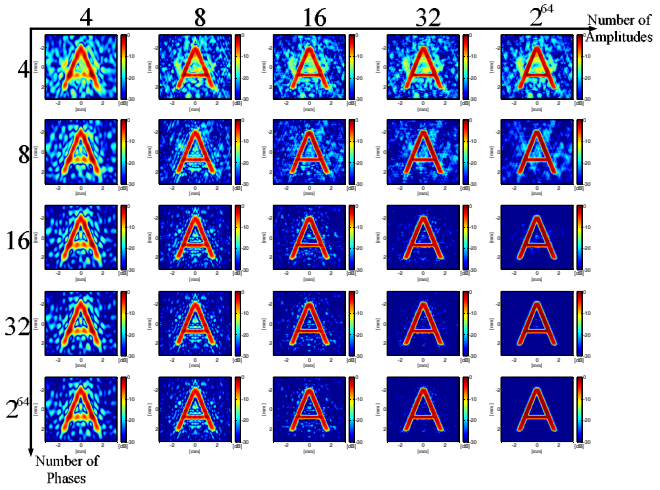

Figure 3. The RMS pressure distribution for the letter "A" with different numbers of quantization levels.

of phases because this combination provides an acceptable image quality while yielding a relatively simpler hardware implementation.

III. Frontend IC Architecture

The main function of the circuit is to generate a burst of unipolar square wave of eight equally spaced amplitude levels and eight uniformly spaced phases. The circuit includes two main parts, a phase generator and a voltage level shifter, which are programmable.

A. Programmable phase generator

The phase generator is designed using a digital approach to maintain minimum area and power dissipation. The input of the phase generator includes four control bits and a clock signal (Fig. 4(a)). The enable bit controls the on/off switching of the phase generator, and the other three control bits (CTRL3, CTRL4, and CTRL5) are used for phase selection. The output is a signal with a frequency, which is ¼ of the input frequency. The phase depends on the phase selection bits. The phase step is $\pi/4$.

B. Programmable voltage level shifter

The programmable voltage level shifter is designed to convert the output signals from the phase generator into square waves of eight equally spaced voltage levels. A modified CMOS inverter is used to generate unipolar square waves (Fig. 4(b)). The level select transistor is used to turn off the charging path after the desired voltage level is reached. The load capacitor represents the net capacitance of the transducer element.

Eight different voltage levels are generated using a resistive divider network. An analog multiplexer is used for amplitude selection. The desired amplitude level is selected using a 3-bit digital input (CTRL0, CTRL1, and CTRL2) for each transducer element.

Although the complexity of the active circuitry in the presented architecture is low, routing the signals of eight

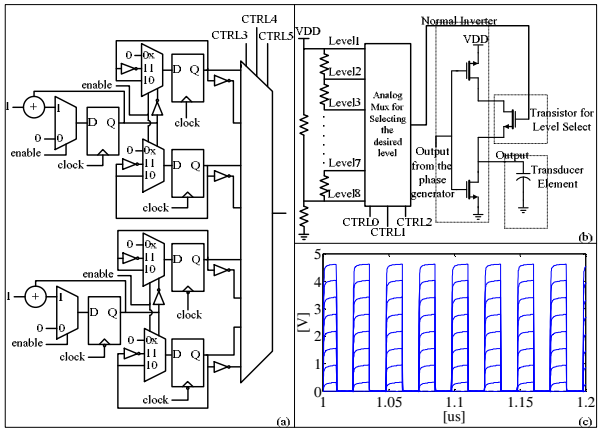

Figure 4. (a) Schematics of the programmable phase generator. (b) Schematics of the programmable voltage level shifter. (c) Square waves generated by the programmable voltage level shifter.

phases and the amplitude references to each element could be challenging.

IV. Simulations and Discussion

A. Simulation results

The twenty-six images of Calibri font letters from "A" to "Z" are used as inputs. Unlike the simulation presented in Section II where the excitation signals are ideal unipolar square waves, in this group of simulations, signals generated by the frontend circuits as simulated at the transistor level are used as the excitation (Fig. 4(c)). The coverage and CNR are used to evaluate the performance of the algorithm.

As a reference, the weighted Gerchberg-Saxton (GSW) algorithm [2] is also tested using the same input parameters but with ideal excitation signals (perfect square waves of arbitrary phases) instead of simulated ones. The RMS pressure distribution from "A" to "C" is shown in Fig. 5. The coverage and CNR curves for the twenty-six letters are shown in Fig. 6 and Fig. 7, respectively.

B. Discussion

In Fig. 5, we can observe that the USFPs generated using the FFT and the GSW algorithm both show good conformity to the original image. However, the USFPs generated by the GSW algorithm appear more granular, while those generated by the FFT projection algorithm look smoother. The coverage and CNR of the FFT projection algorithm are higher than those of the GSW algorithm for all of the twenty-six letters.

Apart from the better performance in coverage and CNR, the FFT algorithm reduces the computational complexity significantly. For an $N \times N$ image, the complexity of its IDFT is $O(N^4)$, while the complexity of its FFT is $O(N^2 \log_2 N)$. For the GSW algorithm, the computational complexity is $O(N^4)$ for each iteration. As the input image becomes more complicated, the number of necessary iterations increases, and the computational load will become even heavier for the GSW algorithm.

One advantage of the GSW algorithm and other approaches

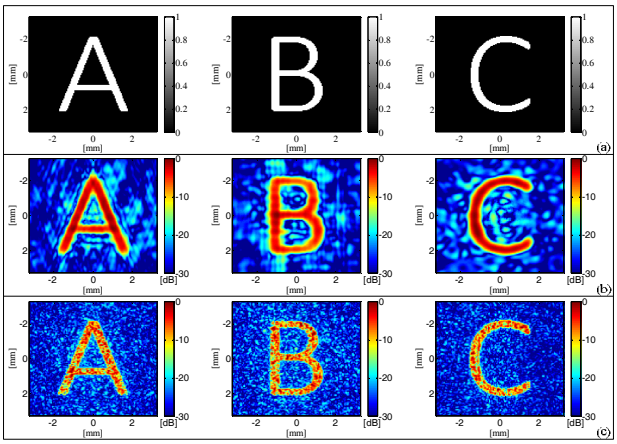

Figure 5. (a) The original image to be projected. The white area is the focused area and the black is the unfocused. (b) Normalized RMS pressure distribution generated using the FFT algorithm with actual excitation signals. (c) Normalized RMS pressure distribution generated using the GSW algorithm with ideal excitation signals.

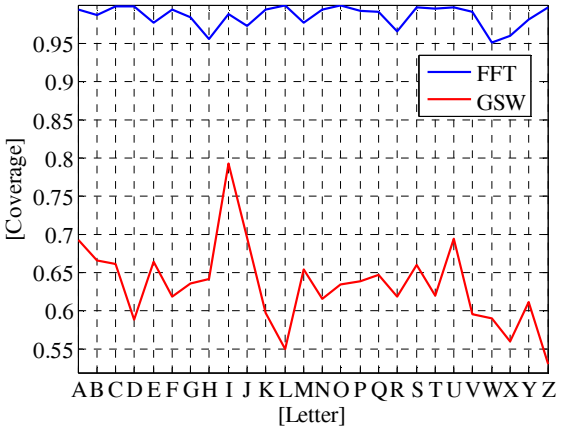

Figure 6. Coverage for FFT and GSW from "A" to "Z"

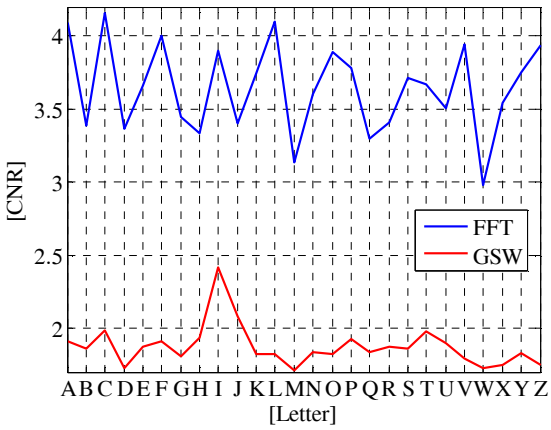

Figure 7. CNR for FFT and GSW from "A" to "Z"

with phase-only focusing is that each transducer element is used at full power capacity (maximal amplitude). However,

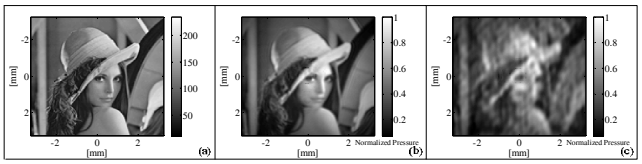

Figure 8. (a) The grayscale image to be projected. (b) The normalized RMS pressure distribution for ideal excitation. (c) The normalized RMS pressure distribution for quantized excitation of eight levels of amplitudes and phases.

the computational complexity for projecting arbitrary images could be prohibitive using these iterative algorithms. For the case presented in this paper, the average pressure in the focused area obtained using the real-time FFT-based algorithm is 11% of the average pressure obtained using the GSW algorithm assuming the same physical array and the same maximum excitation amplitude is used for both. Considering that neural stimulation is performed at relatively low intensity levels, the real-time capability of the presented algorithm would outweigh the described disadvantage of not exciting all elements with maximum amplitude signals.

In the simulations presented in this paper, bit maps were used as the input for more convenient analysis. However, grayscale images can also be used as the input without introducing any changes in computational complexity (Fig. 8). For images resulting in excitation amplitude distributions that are not very uniform, not all quantization levels are equally utilized. Adaptive quantization techniques could be explored to further optimize the presented algorithm.

V. Conclusion

We demonstrated an FFT-based ultrasound projection algorithm that is computationally efficient, and a frontend IC architecture to generate the actual excitation signals for a 2D transducer array. To simplify the hardware implementation, eight levels of amplitudes and phases were used for the quantization of excitation signals. The real-time applicability of the presented approach is its main advantage, which is critical for the retinal stimulation application.

References

[1] M. D. Menz, Ö. Oralkan, P. T. Khuri-Yakub, and S. A. Baccus, "Precise neural stimulation in the retina using focused ultrasound," *J. Neurosci.*, vol.33, no. 10, pp. 4550-60, Mar. 2013.

[2] Y. Hertzberg, O. Naor, A. Volovick, and S. Shoham, "Towards multifocal ultrasonic neural stimulation: pattern generation algorithms," J. Neural Eng., vol. 7, no. 5, p. 056002, Oct. 2010.

[3] J. A. Jensen, "Field: A Program for Simulating Ultrasound Systems," *the 10th Nordic-Baltic Conference on Biomedical Imaging Published in Medical & Biological Engineering & Computing*, vol. 34, supplement 1, part 1, pp. 351-353, 1996.

[4] J. A. Jensen and N. B. Svendsen, "Calculation of pressure fields from arbitrarily shaped, apodized, and excited ultrasound transducers," IEEE *IEEE Trans. Ultrasonics, Ferroelectrics and Frequency Control*, vol. 39, pp. 262-267, 1992.

[5] J. L. Prince and J. M. Links, "Medical Imaging Signals and Systems," Upper Saddle River, NJ: Pearson Prentice Hall, c2006.

[6] P. F. Stetson, F. G. Sommer, and A. Macovski, "Lesion contrast enhancement in medical ultrasound imaging," IEEE Trans. Med. Imag., vol. 16, pp. 416-425, Aug. 1997.